Biosensors and Bioelectronics 182 (2021) 113178

Contents lists available at ScienceDirect

Biosensors and Bioelectronics

journal homepage: http://www.elsevier.com/locate/bios

Engineering a high-efficient DNA amplifier for biosensing application based on perylene decorated Ag microflowers as novel electrochemiluminescence indicators

Fang Yang, Yan-Wei He, Ya-Qin Chai, Ruo Yuan, Ying Zhuo *

Key Laboratory of Luminescence Analysis and Molecular Sensing (Southwest University), Ministry of Education, College of Chemistry and Chemical Engineering, Southwest University, Chongqing, 400715, PR China

ARTICLE INFO

Keywords:
Electrochemiluminescence
DNA amplifier
Perylene decorated Ag microflowers
Biosensor

ABSTRACT

DNA-based amplifiers with high programmability and accurate molecular recognition ability have become a versatile platform for target amplification. However, the random diffusion of capture probes (CPs) in most DNA amplifiers limits the target recognition efficiency, affecting the limit of detection. Herein, a high-efficient DNA amplifier was developed by localizing the CPs consisted of the unique palindromic tails and target recognition sequences on Au nanoparticle modified magnetic beads (Au@MBs). In the presence of target K-ras gene, the CPs with high local concentration and orientation could capture the target efficiently to expose their palindromic tails, which could act as primers to trigger the polymerization for target recycling. More importantly, the polymerization products could involve in the next recycle and produce abundant mimic targets (MTs) continuously, thereby achieving the detection of trace K-ras gene. Meanwhile, a novel electrochemiluminescence (ECL) indicator of a thin-layer of perylene (Pe) molecules decorated Ag microflowers (Pe@Ag MFs) was obtained based on the reaction between the perylene cation radical ($Pe^{\bullet+}$) and Ag atoms. The obtained Pe@Ag MFs exhibited desirable ECL performance because (i) a thin-layer of Pe molecules could reduce the inner filter effect and inactive emitters, (ii) the Ag MFs as coreaction accelerator could react with $S_2O_8^{2-}$ to produce more $SO_4^{\bullet-}$ and shorten the distance between $Pe^{\bullet-}$ and $SO_4^{\bullet-}$ to significantly enhance the ECL intensity of Pe with less energy loss. This work paves the way for the development of efficient amplification strategy and offers a paradigm for the preparation of high-efficiency ECL indicators.

1. Introduction

DNA molecular interactions based on the Watson-Crick base pairing rules have allowed researchers to construct various self-assembled, programmable systems for biological applications (Chen et al., 2017; Zhang et al., 2020a; Bai et al., 2020; Liu et al., 2020; Gao et al., 2020). Especially, the DNA amplifiers with excellent biomolecule transduction and amplification ability have become the driving force for the rapid development of biosensors. For example, Wu's group constructed primer-free strand-displacement amplification (SDA) for gene detection, which overcame the intrinsic drawbacks (such as nonspecific amplification and false positives) of traditional primer-based SDA (Shen et al., 2018). Shin et al., developed an intramolecular SDA by localizing capture probes (CPs) to form a single molecular unit and applied it for miRNA detection (Shin et al., 2019). However, these DNA amplifiers used the randomly diffused CPs to capture the target, which will inevitably bring about low collisional efficiency and unwanted cross-talk reactions, affecting the target recognition efficiency. Recently, Jiang's group developed a relatively motional DNA amplifier between two particles for Zika virus RNA fragments detection (Zhang et al., 2020b). Although the reaction rate in this DNA amplifier was accelerated by increasing local track DNA concentration assembled on Au nanoparticles, the lack of target amplification limited the sensitivity of trace detection. To circumvent these problems, we developed a DNA amplifier in which the CPs with unique palindromic tails and target recognition sequences presented high local concentration and orientation. In the presence of target K-ras gene, the CPs could capture the target efficiently to expose their palindromic tails, which could act as primers to trigger the polymerization for target recycling. More importantly, the polymerization products are able to participate in the next recycle and

* Corresponding author.
E-mail address: yingzhuo@swu.edu.cn (Y. Zhuo).

https://doi.org/10.1016/j.bios.2021.113178
Received 17 December 2020; Received in revised form 16 February 2021; Accepted 17 March 2021
Available online 21 March 2021

produce a large quantity of mimic targets (MTs) continuously, thereby achieving the detection of trace K-ras gene, which is an important member of the ras family and its point mutation could induce the appearance of pancreatic cancer (Forrester et al., 1987).

Polycyclic aromatic hydrocarbons (PAHs) with well chemical stability, high optical gain and easy-processability have been widely used in electrochemiluminescence (ECL) fields (Valenti et al., 2010; Faulkner and Bard, 1968). However, their poor solubility and instability of obtained radical ion in aqueous solution obstructed their further ECL biosensing applications. In recent years, the surfactant-assisted reprecipitation method has been developed to prepare PAHs nanocrystals (NCs) with good stability and enhanced ECL to meet the demand of bioanalysis (Liu et al., 2018; Yang et al., 2018). However, the prepared PAHs NCs presented undesired reproducibility as their morphology and uniformity were easily affected by synthesis conditions (such as the amount of surfactant, reaction time and temperature, etc). In addition, they also had serious inner filter effect and excess inactive emitters due to their dense stacking. Thus, to search for the synthesis method that could control the shape of materials and reduce their inner filter effect is quite necessary. Herein, a semi-sacrificial template method was implemented to synthesize the novel perylene (Pe) molecules decorated Ag microflowers (Pe@Ag MFs) emitters in which Pe molecules (a classical PAH) were used as luminophores and Ag MFs were acted as template. In comparison with Pe NCs prepared by the surfactant-assisted reprecipitation method or the complex of Pe NCs and Ag MFs materials assembled layer by layer, the obtained Pe@Ag MFs not only had a uniform architecture but also exhibited distinctive advantages in ECL performance because (i) a thin-layer of Pe molecules could reduce the inner filter effect and inactive emitters caused by the bulk material, (ii) Ag MFs as coreaction accelerator could react with $S_2O_8^{2-}$ to produce more $SO_4^{\bullet-}$, and shorten the distance between $Pe^{\bullet-}$ and $SO_4^{\bullet-}$ to significantly enhance the ECL intensity of Pe.

In this work, we designed a DNA amplifier as high-efficient target amplification for sensitive detection of K-ras gene based on Pe@Ag MFs as novel ECL indicators. The fabrication mechanism of the biosensor was shown in Scheme 1. Briefly, Pe@Ag MFs were obtained according to the reaction between $Pe^{\bullet+}$ and Ag atoms and then dripped on the glassy carbon electrode (GCE) to form a uniform film (Pe@Ag MFs/GCE) with a strong initial signal. Then, the S1–S2 duplex (S1 modified with thiol and S2 modified with dopamine) as quenching probe was immobilized on Pe@Ag MFs/GCE by Ag–S bond to reduce the background signal enormously. Meanwhile, the CPs with palindromic tails and target recognition sequences were located on the Au nanoparticle modified magnetic beads (Au@MBs) *via* Au–S bond to form the DNA amplifier. Subsequently, the target induced double cycles to produce a large quantity of MTs, which further hybridized with S2 to regain the ECL signal of Pe@Ag MFs, realizing the sensitive detection of K-ras gene.

2. Experimental section

2.1. Preparation of the high-efficient DNA amplifier

Primarily, Au nanoparticles functionalized Fe_3O_4 magnetic beads (Au@MBs) were synthesized according to previously published procedures (see supplementary material for more details). Then, the capture probes (CPs, 4 μM, 200 μL) were mixed with thiol moieties modified S1 (S1-SH, 4 μM, 200 μL) to form the CP-S1 duplexes by annealing at 95 °C for 5 min and cooling down to room temperature. Finally, the CP-S1

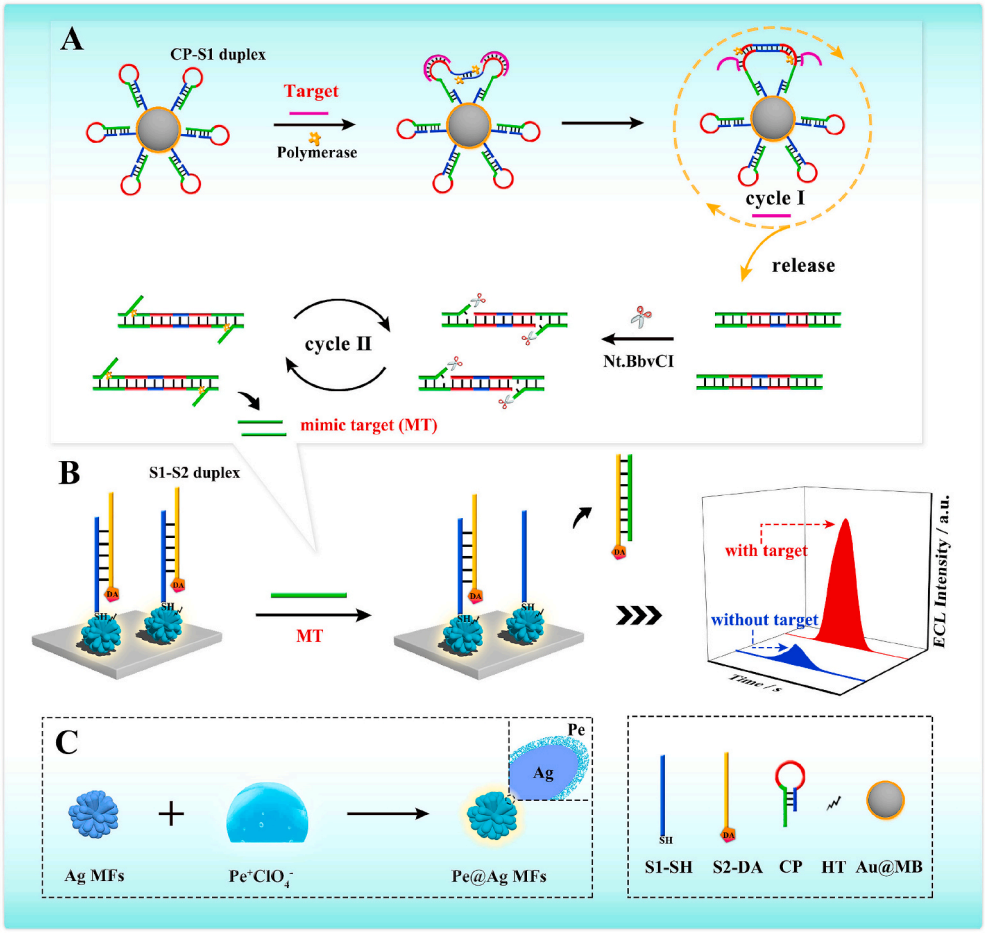

Scheme 1. Work principle of the DNA amplifier (A) and ECL biosensor for K-ras gene detection (B), preparation of Pe@Ag MFs (C).

duplexes were transferred to Au@MBs and reacted overnight at 4 °C to obtain the DNA amplifier through Au–S bond.

2.2. Preparation of Pe@Ag MFs

According to previous report (Lin et al., 2015), the $Pe^{\bullet+}$ could be easily reduced to neutral Pe by Ag atoms. Based on this principle, Pe@Ag MFs were synthesized by introducing $Pe^{\bullet+}$ into the dispersion of Ag MFs. First of all, the $Pe^{\bullet+}$ and Ag MFs were synthesized based on the previous report with some modifications, respectively (see supplementary material for more details). Subsequently, 120 μL of 0.1 mM $Pe^{\bullet+}$ solution in anhydrous acetonitrile was added to 1 mL of 3 mg Ag MFs suspension. After vigorous shaking for 5 min, the color of the Ag MFs suspension turned grayish yellow, indicating the reduction of $Pe^{\bullet+}$ to Pe on the surface of Ag MFs. Finally, the Pe@Ag MFs were separated by centrifugation and washing thoroughly with deionized water.

2.3. Fabrication of the ECL biosensor

To start with, the bare glassy carbon electrode (GCE, $\Phi = 4$ mm) was polished with 0.3 and 0.05 μm alumina oxide slurries, followed by rinsing and sonication with ethanol and deionized water. Then, 5 μL of Pe@Ag MFs suspension was coated on the GCE to form a uniform film (Pe@Ag MFs/GCE). Next, 5 μL of 2 μM S1–S2 duplex, which was prepared by annealing the mixture containing S1-SH and dopamine-modified S2 (S2-DA), was dropped onto the Pe@Ag MFs/GCE for 12 h at 4 °C to obtain the S1–S2 duplex modified GCE (S1–S2/Pe@Ag MFs/GCE) *via* Ag–S bond. Following that, the S1–S2/Pe@Ag MFs/GCE was dipped in 10 μL of hexanethiol (HT, 1 mM) for 1 h at room temperature to obtain HT/S1–S2/Pe@Ag MFs/GCE though Ag–S bond. Finally, the constructed ECL biosensor was rinsed with deionized water and store at 4 °C before to use.

2.4. ECL measurement procedure

First of all, various concentrations of targets were reacted with the DNA amplifier to produce mimic targets (MTs) at different concentrations. Then, the MTs were collected by magnetic separation and transferred to the constructed biosensor. After incubating for 120 min at 37 °C, the biosensor was washed with deionized water and put into an ECL detector cell containing 2 mL of $K_2S_2O_8$ (10 mM, pH 7.4) to record the ECL signal under the potential scanning of −2 to 0 V.

3. Results and discussion

3.1. Characterization of Ag MFs and Pe@Ag MFs

The morphologies of the as prepared Ag MFs and Pe@Ag MFs were investigated by scanning electron microscopy (SEM) and transmission electron microscopy (TEM). It is clearly shown in Fig. 1A that the Ag nanomaterials presented a "flower-like" architecture with diameters from 800 to 1000 nm. Fig. 1B and C were the typical SEM images of the Pe@Ag MFs. It can be seen that the Pe@Ag MFs still displayed the similar architecture and size as that of the prepared Ag MFs. The TEM images of Pe@Ag MFs were shown in Fig. 1D, E and 1F. In the low-resolution TEM image (Fig. 1D), most of the MFs presented uniform

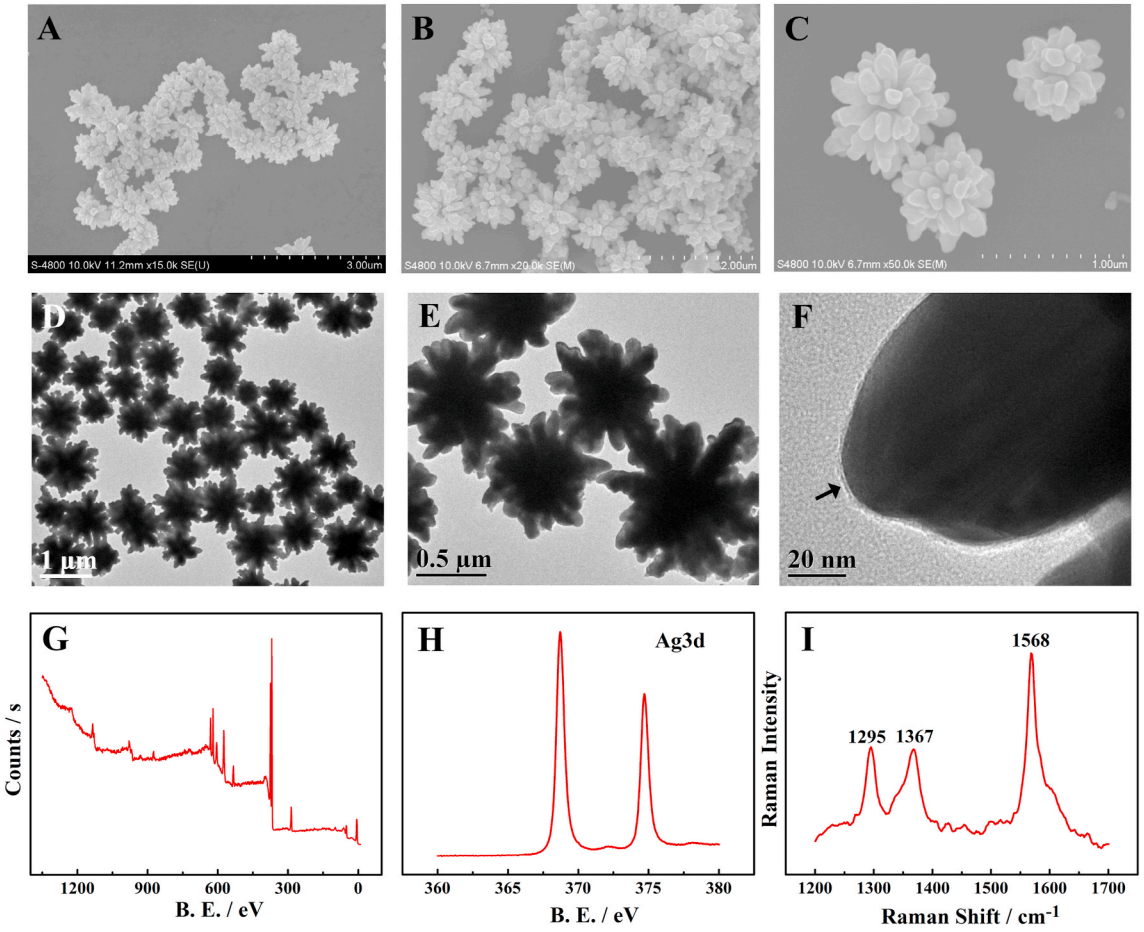

Fig. 1. SEM images of Ag MFs (A) and Pe@Ag MFs (B, C). TEM images of Pe@Ag MFs (D, E, and F). XPS analysis for the full region of Pe@Ag MFs (G), Ag3d regions (H). Raman spectra of Pe@Ag MFs (I).

architecture and good monodispersity. As the resolution increases (Fig. 1E), it can be seen that the Pe@Ag MFs exhibited "flower-like" architecture, comprising of irregular and obtuse branches, which was in line with the SEM observation. Additionally, a layer of Pe molecules could be observed in the high-resolution TEM image of Pe@Ag MFs (Fig. 1F), signifying the formation of Pe@Ag MFs.

The chemical state of Ag in the Pe@Ag MFs sample was investigated by X-ray photoelectron spectrometry (XPS). Fig. 1G shown the full spectra of Pe@Ag MFs sample. From the individual spectral region of Ag3d (Fig. 1H), the binding energy at 368.7 and 374.7 eV were related to $Ag3d_{5/2}$ and $Ag3d_{3/2}$ orbitals, respectively, suggesting the presence of Ag^0 in the sample (Zhou et al., 2013). Besides, Raman intensity of the Pe@Ag MFs sample in the region from 1200 to 1700 cm^{-1} was shown in Fig. 1I. Three bands at 1295, 1367 and 1568 cm^{-1} could be observed, which were similar to the Raman spectrum of Pe molecule in the previous reports (Luo et al., 2008, 2009). In summary, it indicated that the Pe@Ag MFs were synthesized successfully.

3.2. Optical properties of the prepared Pe@Ag MFs

The ECL and photoluminescence (PL) spectra were applied to study the optical properties of the prepared Pe@Ag MFs. The 3D ECL spectra and heat map image (Fig. 2A and B) were used to trace the ECL property of the Pe@Ag MFs from 0 to −2 V and then back to 0 V. From these results, a maximum ECL emission wavelength at 618 nm could be observed. Noticeably, compared with the PL emission spectra (527 nm, Fig. 2C), the maximum ECL emission peak of Pe@Ag MFs showed an obvious red shift ($\Delta\lambda = 91$ nm), implying the formation of excited dimer might be a route for ECL radiation process. (Debad et al., 1996; Fabrizio ete al., 2000).

3.3. The ECL performance of the Pe@Ag MFs

The ECL and electrochemistry performance of different Pe-modified electrodes were investigated using ECL and cyclic voltammetry (CV) techniques. The different Pe-modified electrodes were as follows: (a) Pe nanocrystals (NCs) modified GCE (Pe NCs/GCE), (b) Ag MFs assembled Pe NCs/GCE (Ag MFs/Pe NCs/GCE) and (c) Pe@Ag MFs modified GCE (Pe@Ag MFs/GCE). As depicted in Fig. 3A, the ECL intensity of Pe NCs/GCE was 4192 a.u. After being assembled with Ag MFs, the ECL intensity reached to 8740 a.u. (Fig. 3B), which is about 2.1 times compared to that of Pe NCs/GCE. The reason might be that the Ag MFs as coreaction accelerator could effectively promote the reduction of $S_2O_8^{2-}$ to produce more $SO_4^{\bullet-}$ for enhancing the ECL emission of Pe. Notably, the ECL intensity of Pe@Ag MFs/GCE had increased to 13267 a.u (Fig. 3C). significantly, which is about 3.16 and 1.52 times as much as that of Pe NCs/GCE and Ag MFs/Pe NCs/GCE, respectively. Meanwhile, the Pe@Ag MFs/GCE exhibited the earliest peaking position (6.0 s, curve c, Fig. 3D). The reason for this phenomenon might be that the layer of Pe molecules attached to the surface of Ag MFs could not only reduce the inner filter effect caused by the bulk material, but also shorten the distance between the $Pe^{\bullet-}$ and $SO_4^{\bullet-}$ (produced by the reaction of $S_2O_8^{2-}$ and Ag MFs) to significantly enhance the ECL intensity of Pe with less energy loss. Moreover, the ECL transients spectra of these Pe-modified electrodes were recorded through the step pulse method. As seen in Fig. 3E, the Pe@Ag MFs (curve c) showed the best stability and strongest ECL signal. Furthermore, the ECL relative quantum efficiency of Pe@Ag MFs was ~3.10 and ~1.30 times higher than that of independent Pe NCs and the complex of Pe NCs and Ag MFs materials assembled layer by layer, respectively. (The calculation method and results were shown in the supplementary materials, Table S2). Based on the above discussion, Fig. 3F showed the possible ECL mechanism of the system. In brief, the generation of $SO_4^{\bullet-}$ mainly came from the following two routes: (i) The $S_2O_8^{2-}$ diffused on the electrode surface could generate $SO_4^{\bullet-}$ *via* electroreduction, (ii) Ag MFs as coreaction accelerator could react with $S_2O_8^{2-}$ to produce more $SO_4^{\bullet-}$. Meanwhile, the Pe was reduced to $Pe^{\bullet-}$ under a working potential of −2 to 0 V, which could further become Pe* after reacting with $SO_4^{\bullet-}$. As a result, the Pe* relaxed to the ground state and accompanied by light emission. The possible ECL mechanism of the system was speculated as follows:

$$S_2O_8^{2-} + e^- \rightarrow SO_4^{\bullet-} + SO_4^{2-} \quad (1)$$

$$S_2O_8^{2-} + e^- \xrightarrow{\text{Ag MFs}} SO_4^{\bullet-} + SO_4^{2-} \quad (2)$$

$$Pe + e^- \rightarrow Pe^{\bullet-} \quad (3)$$

$$Pe^{\bullet-} + SO_4^{\bullet-} \rightarrow Pe^* + SO_4^{2-} \quad (4)$$

$$Pe^* \rightarrow Pe + h\nu \quad (5)$$

3.4. Amplification and accelerated effect analysis of the proposed DNA amplifier

To study the amplification and accelerated effect of the developed DNA amplifier. Three modes of DNA amplifiers were constructed and applied to time-dependent ECL analysis. The modes of DNA amplifiers were listed as follows: (a) intermolecular mode, (b) intramolecular mode and (c) localized mode (the proposed DNA amplifier in this work). Fig. 4 revealed that the ECL intensities of these DNA amplifiers were increased with the increment of target incubation time accordingly. Impressively, the ECL intensities of the localized mode (c) were recovered to about 5220 a.u. at 80 min, which was higher than the intermolecular (a, ~3683 a.u.) and intramolecular (b, ~4374 a.u.) modes under the same condition, implying that the proposed DNA amplifier had a good amplification effect. In addition, the ECL intensities of the intermolecular and intramolecular modes reached a plateau at 120 min and 100 min, respectively. While the ECL intensities of the localized mode needed only 80 min to reach a plateau, Moreover, comparing the slopes of the time-dependent ECL curves, the reaction rate of localized mode

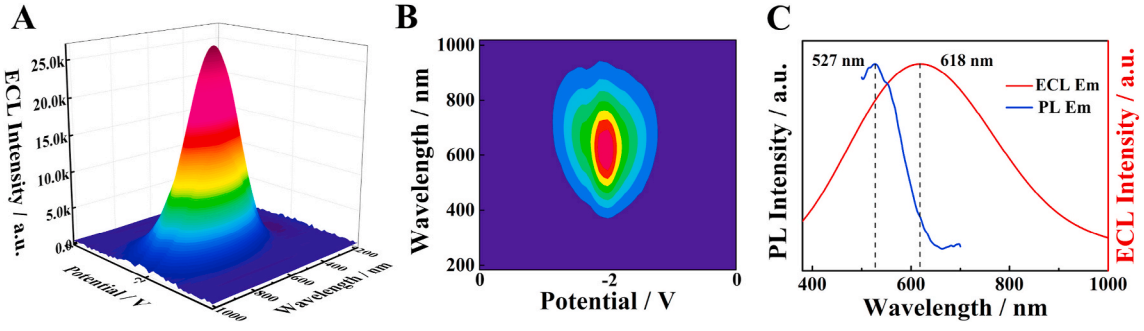

Fig. 2. 3D surface image (A) and heat map image (B) of Pe@Ag MFs. Normalized PL spectra (blue curve) and ECL spectra (red curve) of the Pe@Ag MFs. (For interpretation of the references to color in this figure legend, the reader is referred to the Web version of this article.)

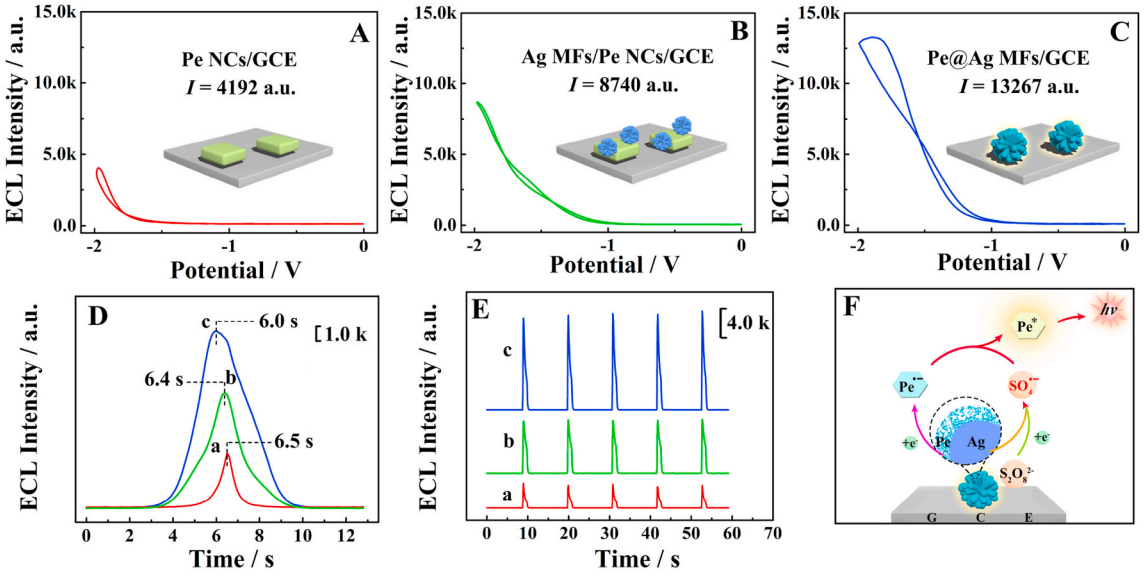

Fig. 3. ECL-potential curves of Pe NCs/GCE (A), Ag MFs/Pe NCs/GCE (B) and Pe@Ag MFs/GCE (C). ECL intensity-time curves (D) and ECL transients (E) of Pe NCs/GCE (curve a), Ag MFs/Pe NCs/GCE (curve b) and (C) Pe@Ag MFs/GCE (curve c), the possible ECL mechanism of system (F).

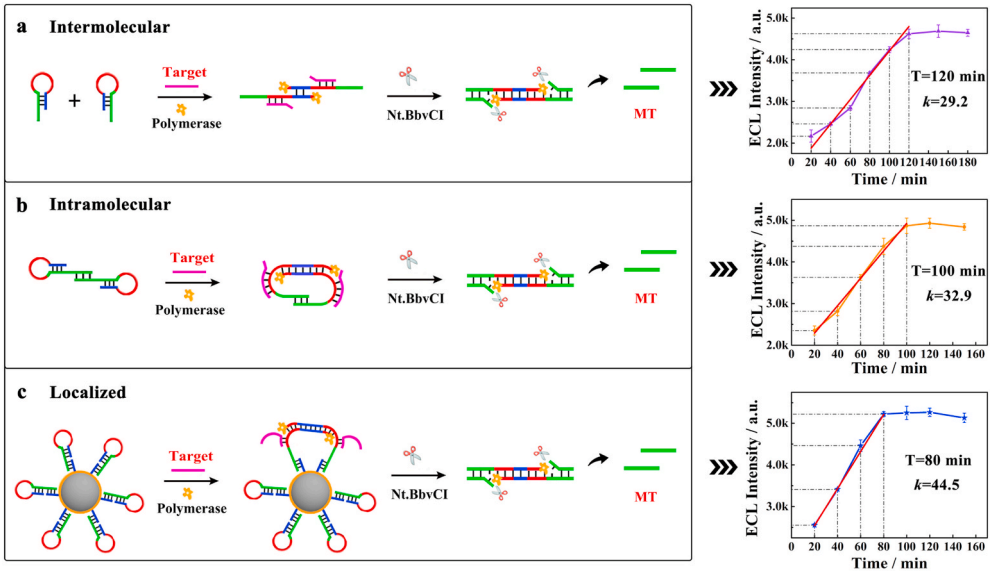

Fig. 4. The work principle and time-dependent ECL analysis of the three modes DNA amplifiers: intermolecular mode (a), intramolecular mode (b) and localized mode (c, the proposed DNA amplifier in this work).

was ~1.52 and ~1.35 times faster than that of intermolecular and intramolecular modes, indicating the higher reaction efficiency of the proposed DNA amplifier. These results obviously demonstrated that the developed DNA amplifier had superior amplification and acceleration effect.

3.5. Analytical performance of the proposed biosensor

After the optimization of the experimental condition (Fig. S3), various concentrations of K-ras gene were tested with the biosensor. As can be seen from Fig. 5A, the obtained ECL intensities increased with the increment of K-ras gene concentrations. This is because the target could be converted into a large number of MTs which further hybridized with the quenching probes to achieve signal recovery. Fig. 5B exhibited that the ECL signals had a good linear relationship with the logarithm of K-ras gene concentrations in the range from 50 fM to 10 nM. According to the linear fitting, the linear equation could be described as $I = 1244.9 \lg c + 4299.3$ ($R = 0.9965$) and the limit of detection (LOD) was computationally determined as 5.1 fM. The biosensor developed in this work had an obvious improvement over other methods in the detection of K-ras gene (Table 1).

Stability was investigated by recording the ECL response towards K-ras gene with the different concentrations ($c = 50$ fM and 10 pM) under continuous potential scanning for 10 cycles. According to Fig. 5C, the ECL response of the biosensor exhibited no obvious fluctuation and the relative standard deviations (RSD) were 1.70% (a) and 1.67% (b), respectively, indicating that the developed biosensor had excellent stability. For specificity investigation, different mismatched DNAs were prepared to replace the target and the corresponding ECL signals were evaluated (Fig. 5D). The relative ECL response of mutant target 1 (MT1), one of the most common mutations of K-ras gene, was about 57.7%. In addition, the relative ECL responses of the mutant target 2 (MT2),

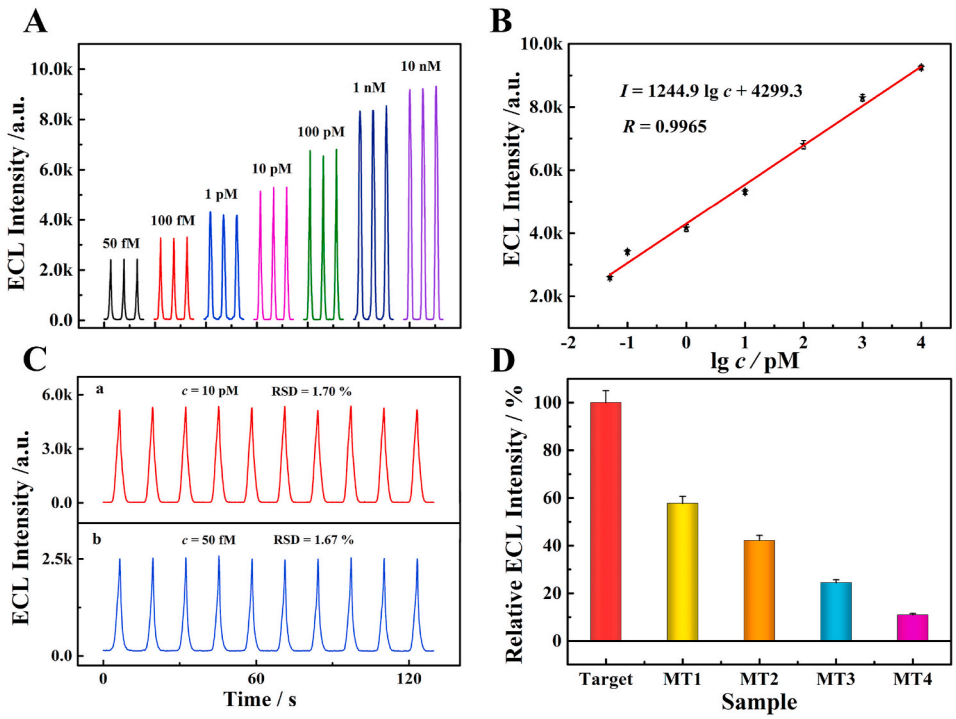

Fig. 5. ECL responses of the developed biosensor towards K-ras gene with different concentrations (A). Calibration curve for the K-ras gene detection (B). Stability curve for 50 fM (a) and 10 pM (b) K-ras gene detection (C), and specificity of biosensor with various mismatched DNAs (D).

Table 1
Comparison of other methods for K-ras gene detection.

Detection	LOD	Linear range	References
Colorimetry	50 pM	100 pM-7 nM	Xu et al. (2017)
FL	10 pM	10 pM-150 nM	Li et al. (2016)
CL	6.0 pM	10 pM-500 nM	Zong et al. (2014)
ECL	30 fM	0.1 pM-1 nM	Zhang et al. (2019)
ECL	5.1 fM	0.05 pM-10 nM	This work

mutant target 3 (MT3), mutant target 4 (MT4) with two, three and four mutation points were about 42.1%, 24.4% and 10.9% respectively. The results indicated that the developed biosensor possessed high detection specificity for target K-ras gene.

4. Conclusion

To sum up, a sensitive K-ras gene biosensor was constructed by using the Pe@Ag MFs as ECL emitters and high-efficient DNA amplifier as target amplification. Compared with the traditional DNA amplifiers with randomly diffused CPs, the proposed DNA amplifier exhibited outstanding advantages in terms of target recognition thanks to the location of CPs. In addition, Pe@Ag MFs showed excellent ECL performance because (i) a thin layer of Pe molecules could reduce the inner filter effect and inactive emitters, (ii) the Ag MFs could accelerate the reduction of coreactant $S_2O_8^{2-}$ to generate plentiful reaction intermediate $SO_4^{\bullet-}$, and shorten the distance between $Pe^{\bullet-}$ and $SO_4^{\bullet-}$ to significantly enhance the ECL intensity of Pe with less energy loss. Taking of these advantages, we believe that the developed biosensor holds great potential in trace biomarker detection with high-efficiency and could be further applied in early clinical diagnostics.

CRediT authorship contribution statement

Fang Yang: Conceptualization, Methodology, Investigation, Formal analysis, Writing – original draft. **Yan-Wei He:** Investigation, Formal analysis. **Ya-Qin Chai:** Methodology, Resources. **Ruo Yuan:** Methodology, Resources. **Ying Zhuo:** Supervision, Methodology, Resources, Writing – review & editing, Project administration, Funding acquisition.

Declaration of competing interest

The authors declare that they have no known competing financial interests or personal relationships that could have appeared to influence the work reported in this paper.

Acknowledges

This work was financially supported by the NNSF of China (22022408), the Chongqing Talents Personnel Support Program (CQYC201905067), the Fundamental Research Funds for the Central Universities (XDJK2019TJ002).

Appendix A. Supplementary data

Supplementary data to this article can be found online at https://doi.org/10.1016/j.bios.2021.113178.

References

Bai, M., Chen, F., Cao, X.W., Zhao, Y., Xue, J., Yu, X., Fan, C.H., Zhao, Y.X., 2020. Angew. Chem. Int. Ed. 59, 13267–13272.
Chen, F., Bai, M., Cao, K., Zhao, Y., Cao, X.W., Wei, J., Wu, N., Li, J., Wang, L.H., Fan, C. H., Zhao, Y.X., 2017. ACS Nano 11, 11908–11914.
Debad, J.D., Morris, J.C., Lynch, V., Magnus, P., Bard, A.J., 1996. J. Am. Chem. Soc. 118, 2374–2379.
Fabrizio, E.F., Prieto, I., Bard, A.J., 2000. J. Am. Chem. Soc. 122, 4996–4997.
Faulkner, L.R., Bard, A.J., 1968. J. Am. Chem. Soc. 90, 6284–6290.
Forrester, K., Almoguera, C., Han, K.Y., Grizzle, W.E., Perucho, M., 1987. Nature 327, 298e303.
Gao, X., Niu, S., Ge, J., Luan, Q., Jie, G., 2020. Biosens. Bioelectron. 147, 111778.
Li, N., Hao, X., Kang, B.H., Xu, Z., Shi, Y., Li, N.B., Luo, H.Q., 2016. Biosens. Bioelectron. 77, 525–529.
Lin, L., Gao, G.Q., Zhu, Q., Xu, A.W., 2015. J. Mater. Chem. A 3, 12845–12851.
Liu, J.L., Tang, Z.L., Zhang, J.Q., Chai, Y.Q., Zhuo, Y., Yuan, R., 2018. Anal. Chem. 90, 5298–5305.

Liu, Z., Lei, S., Zou, L., Li, G., Xu, L., Ye, B., 2020. Biosens. Bioelectron. 147, 111759.
Luo, Z., Luo, Y., Li, J., Liu, K., Fu, H., Ma, Y., Yao, J., 2009. Chem. Commun. 11, 1342–1344.
Luo, Z., Peng, A., Fu, H., Ma, Y., Yao, J., Loo, B.H., 2008. J. Mater. Chem. 18, 133–138.
Shen, Z.F., Li, F., Jiang, Y.F., Chen, C., Xu, H., Li, C.C., Wu, Z.S., 2018. Anal. Chem. 90, 3335–3340.
Shin, S.W., Ahn, S.Y., Lim, Y.T., Um, S.H., 2019. Anal. Chem. 91, 14808–14811.
Valenti, G., Bruno, C., Rapino, S., Fiorani, A., Jackson, E.A., Scott, L.T., Marcaccio, M., 2010. J. Phys. Chem. C 114, 19467–19472.
Xu, H., Wu, D., Li, C.Q., Lu, Z., Liao, X.Y., Huang, J., Wu, Z.S., 2017. Biosens. Bioelectron. 90, 314–320.
Yang, S.S., Jiang, M.H., Chai, Y.Q., Yuan, R., Zhuo, Y., 2018. ACS Appl. Mater. Interfaces 10, 38648–38655.
Zhang, H., Xu, X., Jiang, W., 2020a. Chem. Sci. 11, 7415–7423.
Zhang, Y., Wang, W., Lin, Z., Liu, B., Zhou, X., 2020b. Biosens. Bioelectron. 161, 112256.
Zhang, Q., Liu, Y.Y., Nie, Y.X., Yang, L., Ma, Q., 2019. Anal. Chem. 91, 13780–13786.
Zhou, Y., Yang, J., He, T., Shi, H., Cheng, X., Lu, Y., 2013. Small 9, 3445–3454.
Zong, C., Wu, J., Liu, M.M., Yang, L.L., Liu, L., Yan, F., Ju, H.X., 2014. Anal. Chem. 86, 5573–5578.